DESIGN OF A FULL ETCH GRATING COUPLER

A Thesis

by

TYLER ERNEST BRAVO

Submitted to the Office of Graduate and Professional Studies of
Texas A&M University
in partial fulfillment of the requirements for the degree of

MASTER OF SCIENCE

Chair of Committee,	Christi Madsen
Committee Members,	Ohannes Eknoyan
	Gregory Huff
	Alexey Belyanin
Head of Department,	Miroslav Begovic

May 2017

Major Subject: Electrical Engineering

ABSTRACT

The design of a full etch, constant pitch grating coupler with upper oxide cladding is documented and analyzed for coupling to the dominant TE mode of a waveguide on a commercially available SOI platform at 1550nm. A high level design approach using Fresnel reflection theory, waveguide mode theory, and wave interference principles is used to develop a parametric model of the grating coupler, and this model is tested and analyzed using a rigorous coupled mode analysis engine contained within the FIMMWAVE software package. To automate testing and analysis of the high level grating model, a GUI plugin to FIMMWAVE was also developed using Python's PyQT package.

It will be shown that this high level, "Device Modes" modelling process is very capable of describing specific optical behaviors of the grating structure, and is also very capable of producing efficient couplers. Simulated coupling efficiencies between the grating waveguide's dominant mode and single mode fiber reach as high as -3.55 dB at 1550nm for this full etch, constant pitch design. This methodology is easily adapted to different index profiles, and when coupled with its minimum of fabrication complexity will allow quick access to a coupling technology for novel photonic integrated circuit platforms.

CONTRIBUTORS AND FUNDING SOURCES

Contributors

This work was supervised by a thesis committee consisting of Professors Christi Madsen, Ohannes Eknoyan, and Gregory Huff of the Department of Electrical and Computer Engineering, and Professor Alexey Belyanin of the Department of Physics.

All work for the thesis was completed independently by the student.

Funding Sources

This work was made possible in part by the AFRL Research Collaboration Program under Grant Number FA8650-13-C-5800. Its contents are solely the responsibility of the authors and do not necessarily represent the official views of the AFRL.

TABLE OF CONTENTS

Page

LIST OF FIGURES

Page

LIST OF TABLES

Page

1. INTRODUCTION

Grating couplers are an enabling technology for the research and development of photonic integrated circuits (PICs). From a fabrication standpoint, a grating coupler can be as complex or as simple as the designer wants, but there are obvious efficiency tradeoffs for opting for the simple-to-fabricate. While complex design nodes may lend the designer more control over coupling efficiency, they also require more advanced processing steps that can make them inapplicable to less developed integrated photonics platforms. For this reason, a straightforward method for designing an efficient, full etch, constant pitch grating coupler will be presented. The fabrication simplicity will allow for novel PIC platforms to have quick access to a coupling technology, and it will also allow for less advanced fabrication operations to build their own structures on common PIC platforms. We will employ this methodology to design a grating coupler for a commercially available SOI platform from SOITEC, and then verify the design using a rigorous coupled mode analysis engine from FIMMWAVE. In what follows, the bounds of the design example will be framed in a design statement, and some basic theory and strategy regarding the high level design approach will be introduced.

1.1 Design Statement

The focus of this design problem is encapsulated by the following statement: "Develop an efficient grating coupler design for a commercially available SOI platform that requires a minimum of processing complexity." By starting with a commercially available SOI platform, we will reduce fabrication time and also reduce fabrication error, as the manufacturing tolerances of an automated, commercial operation are likely orders

of magnitude better than what can be achieved in a research fab. Our design will thus be limited by the bounds for thickness of the buried oxide layer and top layer silicon that the company provides.

After acquiring the SOI platform, we will seek to pin the remaining processing steps to a minimum of quantity and complexity. To achieve this end, we will force our design to be full etch and constant pitch. To improve coupling efficiency, our design will also account for an upper cladding of SiO_2, which will have the secondary benefit of providing a protective layer to the Si cored PICs on the remainder of the chip. The post processing steps after platform acquisition are thus limited to a single full etch of the top layer silicon, and a single oxide growth or deposition process.

Further limitations to the design will be to keep the top layer silicon at a thickness that single-mode operation will be achievable by waveguide circuitry on the remainder of the chip. We will also assert operation at 1550nm with TE polarization. The basic structure and design parameters are shown in figure 1.1 for reference, and will be expounded upon in section 2.1.

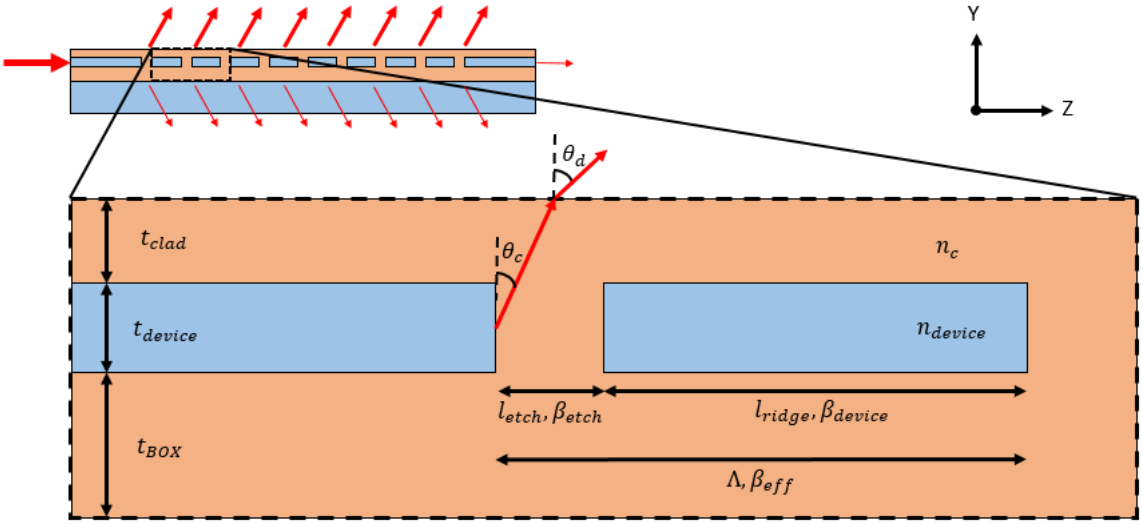

Figure 1.1: Generalized Cross Section of Grating Device

1.2 Design Approach

Reference	Coupling Efficiency	Notes
[1]	$-4.8\ dB$	TE; Variable pitch; No cladding; Genetic algorithm to optimize BOX thickness
[2]	$-1.8\ dB$	TE; Variable pitch; No cladding; Photonic crystal based
[3]	$-4\ dB$	TM; Constant Pitch; No cladding; Interleaved full etch
[4]	$-3.47\ dB$	TE; Constant Pitch; With cladding; Particle swarm optimization for cladding thickness
[5]	$-1.91\ dB$	TE; Variable pitch; With cladding; Particle swarm optimization for BOX and cladding thickness

Table 1.1: Literature Report on Simulated Results for Full Etch SOI Gratings

A sample of simulation results ranging into the state-of-the-art in fully etched SOI gratings is compiled in table 1.1. Their peak coupling efficiencies range from -1.74 to -4 dB, but none of them are strictly full etch and constant pitch, and a few of them do not have upper claddings. Many of them also rely on heavy computational optimization

routines to determine specific device parameters. The design approach presented in this paper is meant to bypass these heavy optimization routines, or to augment them by providing a base level of intelligence about the efficiency behavior of a grating.

To develop our model for this grating, we will examine a small subset of fields around the grating structure that are high impact for the process of converting a guided mode in the device layer to a Gaussian mode propagating up and away from the composite structure. Each of these fields will have an associated k-space that is able to tell us the relative phase between two points in the field, and we will use this feature to assert a set of beneficial resonance conditions that are functions of the device's geometry. These resonance conditions will be modal by nature, as they will be assertions that a sum or a difference of phase be equal to, for example, $2\pi m$ for constructive interference, or $2\pi m - \pi$ for destructive interference. Solving this set of equations for integer values of the phase parameters (the "m" in each of these equations) will deliver to us a device that mathematically achieves these beneficial resonances; but, we will see that not all of these integer "device modes" will be real devices, nor will they all necessarily achieve the resonant behavior we have set out for them.

For example, a non-real device mode might be one that has a negative value for etch length. On the other hand, a device mode that is real but that definitely will not achieve the resonant behavior we want is one that has too long an etch length – all the power would radiate from the first aperture in the grating, and we would not get the desired "phased array" effect. Due to the presence of these undesirable device modes, it will then be incumbent upon us to filter down to the device modes that contain real

devices, and then to the device modes that contain structures that enable our resonance conditions.

The high level concepts required for this design process include k-space, for tracking the relative phase of an oscillating field through spatial coordinates, and Fresnel reflection, for accounting for phase shifts of a field on reflection. These concepts will be applied to track the relative phase of the plane-wave and guided-wave fields present in and around a grating structure, and will allow us to develop the aforementioned set of equations.

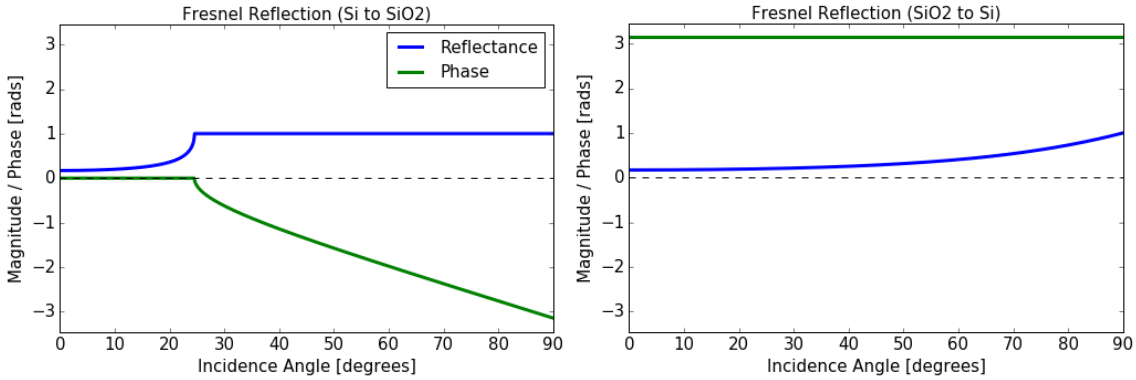

Figure 1.2: Fresnel Reflection at TE Incidence

$$r_{TE}(n_i, n_t, \theta_i) = \frac{n_i \cos(\theta_i) - n_t \sqrt{1 - \left(\frac{n_i}{n_t}\sin(\theta_i)\right)^2}}{n_i \cos(\theta_i) + n_t \sqrt{1 - \left(\frac{n_i}{n_t}\sin(\theta_i)\right)^2}} \qquad (Equation\ 1.1)$$

$$\phi_{r,TE} = \angle(r_{TE}) \qquad (Equation\ 1.2)$$

$$R_{TE} = |r_{TE}|^2 \qquad (Equation\ 1.3)$$

In figure 1.2, Fresnel reflection at TE incidence is graphed for incidence at both sides of a Si-SiO_2 interface. The key takeaway here is that reflection from a high-to-low (Si to SiO_2) index transition will undergo a varying phase shift only during total internal reflection (TIR), while reflection from a low-to-high index transition will undergo a constant phase shift of π for all angles of incidence. The TIR phase shift will have large ramifications for calculating the propagation constant of guided modes in the device layer, while the low-to-high index phase shift will have large ramifications for determining cladding and BOX layer thicknesses. Equation 1.1 documents the complex reflection coefficient for TE incidence. The complex angle of this coefficient gives the phase shift (Equation 1.2), while the magnitude squared gives the fraction of incident power reflected, or the reflectance (Equation 1.3).

2. FULL ETCH GRATING MODEL

Following the constraints laid out in the design statement subsection, and the process laid out in the design approach subsection, we can proceed with the design of our grating coupler. First, we will define the device geometry. Then, we will identify what phase matching goals will be most beneficial to us. Finally, we will derive the grating model equations by tracing specific paths through the associated fields and accounting for phase as we go.

2.1 Device Geometry

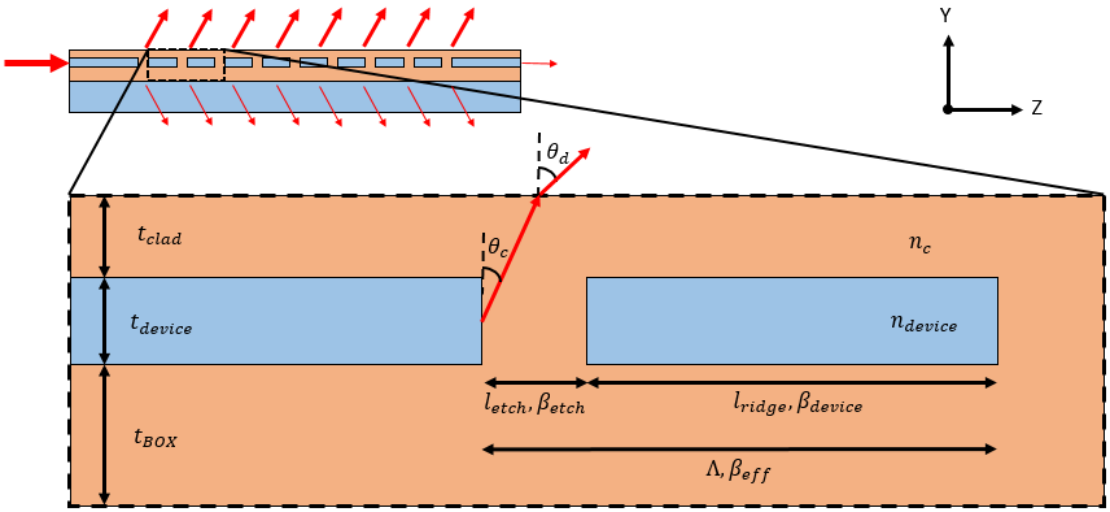

Figure 2.1: Device Geometry Cutaway

A two-period cutaway of the full etch, constant pitch grating with top cladding oxide is depicted in figure 2.1. Specific references to Si and SiO_2 indexes are not included in the graphic to highlight that the design is not dependent on that specific material composition. For our device however, the blue regions will identify Si, while the orange regions will identify SiO_2. The refractive index of Si is labelled as n_{device},

and the refractive index of SiO_2 is labelled as n_c. The subscript assignment in n_c follows from the top cladding and the buried oxide layer serving as a collective cladding to the device layer waveguide segments.

The cutaway also identifies thicknesses for the buried oxide layer, the periodically etched device layer, and the top cladding layer. These are t_{BOX}, t_{device}, and t_{clad}, respectively. The constant etch length is also identified as l_{etch}, and this etched segment occurs periodically with period length Λ. The remaining length of each period, which identifies the length of un-etched silicon in the device layer, is named l_{ridge}.

Also important to note are the propagation constants of the device layer's waveguide and etch segments, β_{device} and β_{etch}. The propagation constants are intended to track the relative phase of the dominant mode as it propagates from one waveguide segment to the next in the z-direction, so they are very important for setting the cladding out-radiation angle θ_c. β_{device} *is* the dominant propagating mode of the Si device layer, so it is a function of device layer thickness. It will always be less than the plane wave propagation constant in Si, and greater than the plane wave propagation constant in SiO_2; i.e., it will always be less than k_{device}, and greater than k_c. On the other hand, it is noteworthy to consider that β_{etch} might not be as straightforward a parameter to come to. In a partial etch grating, β_{etch} would simply be determined by the composition and thickness of the remaining waveguide in the etched region, but in a full etch grating there is no similar guiding structure. We will instead approximate that the propagation constant β_{etch} is always equal to the plane wave propagation constant in the cladding region, k_c.

To make calculations cleaner, we can also identify an effective propagation constant, β_{eff}, to account for the phase accumulated over one period of our grating. Since β_{device} and β_{etch} are the same for each period in our grating, and l_{ridge} and l_{etch} are likewise the same, the total phase accumulated over each period will also be the same. β_{eff} can then be used to account for the phase accumulated along the length of the grating region, but only if the length that β_{eff} is multiplied by is a multiple of the period length Λ.

Equation 1.4 shows the equivalence of the explicit and the effective formulations for the phase gained through one period of the grating, denoted as ϕ_{period}. Equation 1.5 defines β_{eff} in terms of the segment-wise propagation constants β_{device} and β_{etch}, and also of a new term named fill factor (ff). Fill factor is then simply defined as the fraction of one period that is etched (Equation 1.6).

$$\phi_{period} = \beta_{device} l_{ridge} + \beta_{etch} l_{etch} = \beta_{eff} \Lambda \qquad (Equation\ 1.4)$$

$$\beta_{eff} = \beta_{device}(1 - ff) + \beta_{etch}(ff) \qquad (Equation\ 1.5)$$

$$ff = \frac{l_{etch}}{\Lambda} \qquad (Equation\ 1.6)$$

2.2 Phase Matching Goals

We will now identify a set of phase matching goals that, when satisfied, will contribute to the potential for our device to resonate in a manner that is beneficial for coupling. We use the language, 'potential to resonate' due to the fact that we are only going to focus on optimizing the grating geometry for a small subset of the fields around

the device. If we can satisfy enough of these resonance conditions simultaneously, then we will see that the cumulative behavior we are searching for will be manifest.

Condition	Desired Behavior	Phase Function	Desired Result
Grating Out-Radiation	Coherent for θ_c	$M(\theta_c, \beta_{eff}, \Lambda)$	$2\pi m$
Grating Back-Reflection	Incoherent	$N(\beta_{eff}, \Lambda)$	$2\pi n - \pi$
Cladding Resonance	Maximized for θ_c	$P(\theta_c, t_{clad})$	$2\pi p$
BOX Resonance	Minimized for θ_c	$Q(\theta_c, t_{BOX})$	$2\pi q - \pi$
Composite Radiation Bias	Upward coherence for θ_c	$F(\theta_c, t_{device}, t_{BOX})$	$2\pi f$

Table 2.1: Phase Matching Goals

Table 2.1 identifies our set of five resonance conditions. Many of their results are guided by a chosen cladding de-coupling angle, θ_c. This θ_c is related to the free space de-coupling angle θ_d by Snell's law. In the following subsections, we will derive the governing phase tracking functions *M*, *N*, *P*, *Q*, and *F* for each of these resonance conditions. We will see that for a selected θ_c, if we set the phase parameters *m*, *n*, *p*, *q*, and *f* to integer values, then we will be able to solve the resulting system of equations to fully define our grating structure. Since integer values of the phase parameters correspond to a resonance behavior that is defined to benefit coherent radiation at θ_d from the top surface of the structure, devices designed in this way should provide promising results.

However, as mentioned in the design approach subsection of the introduction, these "*mnpqf* device modes" will not all contain valid devices. Some device mode solutions will turn out devices with negative etch lengths, or some other mode solutions might not satisfy some implicit dependency of our phase tracking functions. The primary dependency culprit here will be the grating out-radiation condition, which is

dependent on there being radiation from each of the successive etched apertures in the grating structure. If the etch length is too long, then most of the power will be radiated out of the first aperture, and the phased array effect accounted for in the grating out-radiation equation will not hold.

In the remainder of section 2, we will determine the form of each of these *M*, *N*, *P*, *Q*, and *F* phase tracking functions, and in section 3 we will explore how to filter the compiled model to valid solutions.

2.3 Grating Out-Radiation

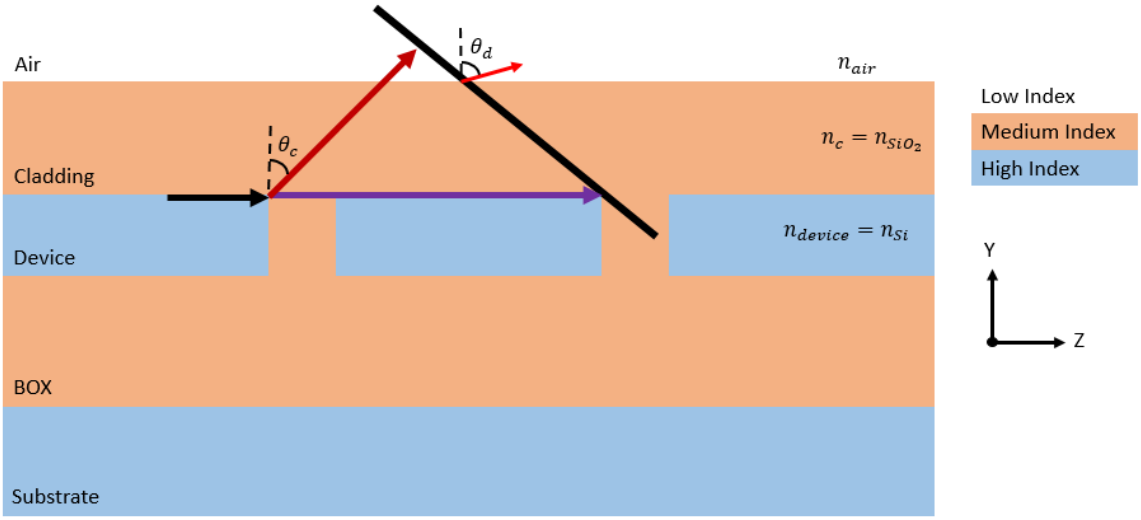

Figure 2.2: Grating Out-Radiation Diagram
Grating out-radiation angle is asserted by setting a specific phase relationship between successive apertures of the grating.

$$M(\theta_c, \beta_{eff}, \Lambda) = 2\pi m \qquad (Equation\ 2.1)$$

$$M(\theta_c, \beta_{eff}, \Lambda) = \phi_{grating} - \phi_{radiation} \qquad (Equation\ 2.2)$$

$$M(\theta_c, \beta_{eff}, \Lambda) = \beta_{eff}\Lambda - k_c \sin(\theta_c)\,\Lambda \qquad (Equation\ 2.3)$$

This resonance condition serves to maximize the power in a given radiation mode, and is driven by setting the phase difference between each of the radiating apertures in the grating such that they are in phase with a plane wave propagating at angle θ_c. In figure 2.2, the phase accumulated over the purple path is $\phi_{grating} = \beta_{eff}\Lambda$, while the phase accumulated over the red path is $\phi_{radiation} = k_c \sin(\theta_c)\,\Lambda$. The angle θ_c determines the plane wave propagation angle, and $\Lambda \sin(\theta_c)$ is the distance from the first aperture to a plane wave-front that intersects the second aperture. We want the phase difference accumulated between these two paths to be a multiple of $2\pi m$ so that they constructively interfere and carry on propagating in θ_c. Since the grating structure is periodic, this condition will hold for each subsequent aperture as long as the etch length is sufficiently short. If the etch length is short enough, the subsequent apertures will receive power from the dominant mode of the previous device layer waveguide, and this resonance condition will hold. Note that the plane wave at angle θ_c in the cladding will de-couple into a free space plane wave at angle θ_d that can be calculated from Snell's Law.

2.4 Grating Back-Reflection

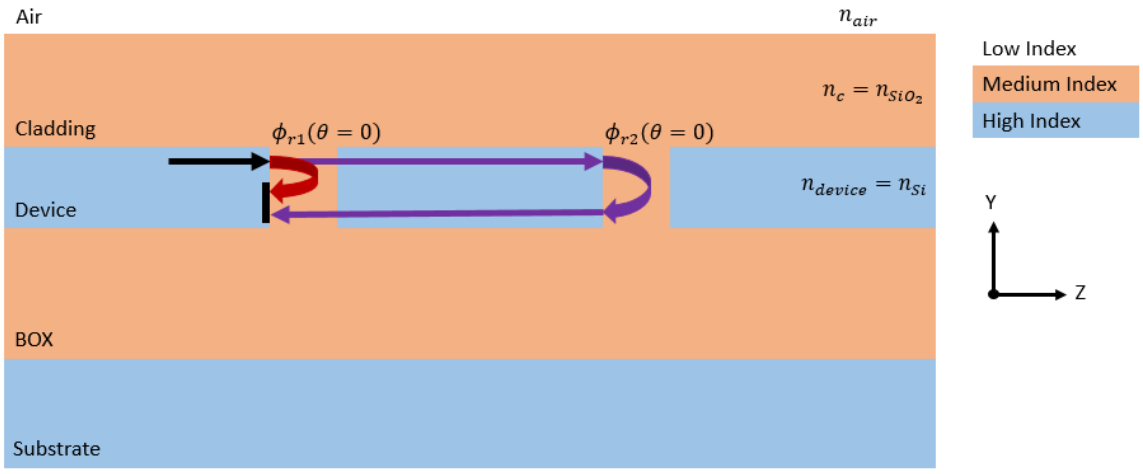

Figure 2.3: Grating Back-Reflection Diagram
Back reflection is minimized by asserting that successive reflections are out of phase.

$$N(\beta_{eff}, \Lambda) = 2\pi n - \pi \qquad (Equation\ 2.4)$$

$$N(\beta_{eff}, \Lambda) = \phi_{R2} - \phi_{R1} \qquad (Equation\ 2.5)$$

$$N(\beta_{eff}, \Lambda) = 2\beta_{eff}\Lambda + \phi_{r2} - \phi_{r1} \qquad (Equation\ 2.6)$$

$$N(\beta_{eff}, \Lambda) = 2\beta_{eff}\Lambda \qquad (Equation\ 2.7)$$

To minimize grating back-reflection, we need to assert that successive reflections of the guided mode from the etched interfaces will be out of phase with each other. We will assert this for interfaces that are Λ apart (two etch regions), rather than for the successive interfaces in a single etch region. This is accomplished by setting the phase difference between the purple path (ϕ_{R2}) and the red path (ϕ_{R1}) in figure 2.3 to a half multiple of 2π ($i.e.\ 2\pi n - \pi$). The phase gained due to Fresnel reflection is denoted as ϕ_{r1} for the purple path, and ϕ_{r2} for the red path. It is noteworthy that the expression for $N(\beta_{eff}, \Lambda)$ can be formulated for the set of interfaces at the beginning or at the end of

two consecutive etch regions. The expression will hold for either case, as the phase gained from the reflections is the same in both cases, and therefore cancels.

2.5 Cladding Resonance

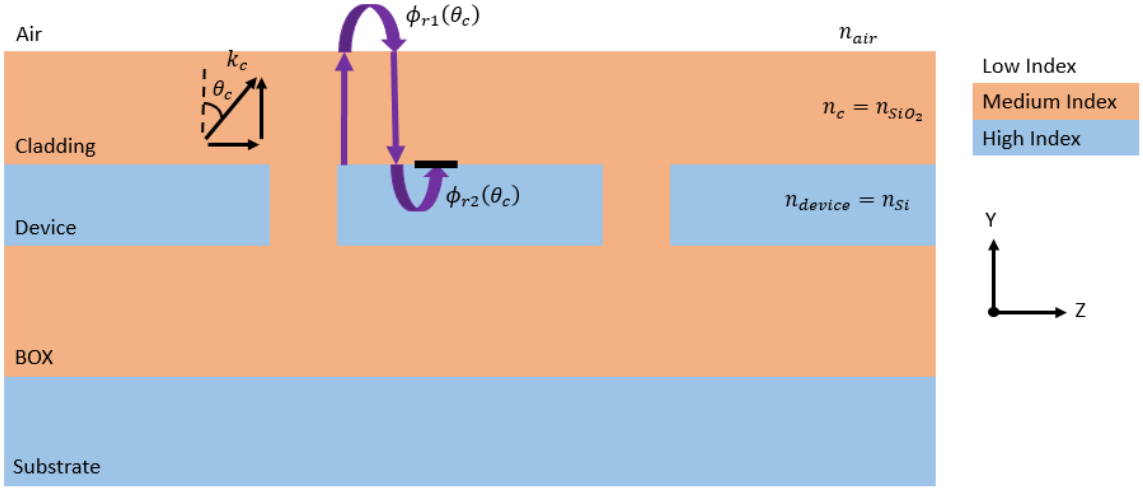

Figure 2.4: Cladding Resonance Diagram
Upwards transmission maximized by asserting a self-supporting leaky mode at θ_c in the top cladding.

$$P(\theta_c, t_{clad}) = 2\pi p \qquad (Equation\ 2.8)$$

$$P(\theta_c, t_{clad}) = 2k_c \cos(\theta_c)\, t_{clad} + \phi_{r1}(\theta_c) + \phi_{r2}(\theta_c) \qquad (Equation\ 2.9)$$

$$P(\theta_c, t_{clad}) = 2k_c \cos(\theta_c)\, t_{clad} + \pi \qquad (Equation\ 2.10)$$

If the grating out-radiation condition is met, a radiation mode will be propagating through the upper cladding at an angle θ_c. The thickness of the upper cladding can have a positive or a negative impact on how much of this radiation mode actually makes it out of the device and in to free-space. We can use waveguide mode theory to understand that at a certain thickness, reflections from the upper and lower interfaces of the top cladding will be self-supporting. However, we also know that there is not total internal reflection occurring at the cladding-air interface (due to angle θ_c being too small), nor

the cladding-silicon interface (due to low-to-high index contrast), so even with a self-supporting thickness the mode will be leaky and will radiate. Since this leaky mode is the primary field that links our free space plane wave mode and our device layer guided mode, we want to boost its resonance so that it draws the most power. Therefore, we will assert that it is a self-supporting mode with a multiple of 2π in phase gained from a round trip.

Another way of understanding this is from a thin film reflection and transmission standpoint. From Figure 2.4, if there is a multiple of 2π phase shift after traversing the entire purple path, then it means that after reflection ϕ_{r2}, the wave is in phase with the initially incident wave, and transmission through the layer will be at a peak. In the end, the phase matching condition for maximized thin film transmission at θ_c is the same as the phase matching condition for creating max resonance in a leaky mode at θ_c.

Note that in phase tracking function P, ϕ_{r1} does not contribute any phase due to it being a non-TIR reflection at a high-to-low index interface, while ϕ_{r2} contributes a π phase shift due to it being a reflection at a low-to-high index interface. θ_c is not a TIR angle by design, because if it were our radiation mode would not transmit into free space.

2.6 BOX Resonance

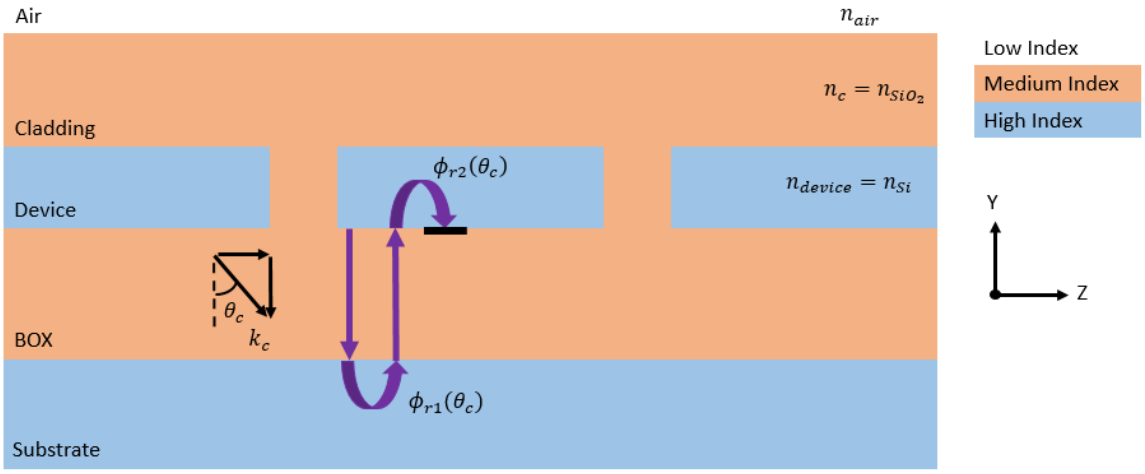

Figure 2.5: BOX Resonance Diagram
Downward transmission minimized by asserting a self-destructing leaky mode in the buried oxide layer.

$$Q(\theta_c, t_{BOX}) = 2\pi q - \pi \qquad (Equation\ 2.11)$$

$$Q(\theta_c, t_{BOX}) = 2k_c \cos(\theta_c)\, t_{BOX} + \phi_{r1}(\theta_c) + \phi_{r2}(\theta_c) \qquad (Equation\ 2.12)$$

$$Q(\theta_c, t_{BOX}) = 2k_c \cos(\theta_c)\, t_{BOX} + 2\pi \qquad (Equation\ 2.13)$$

The BOX resonance condition is very similar to the cladding resonance condition, but we want to lower the resonance of the leaky BOX mode rather than raise it, thus causing it to draw less power. From a thin film transmission and reflection standpoint, the successive reflections will be out of phase with the initially incident, downward propagating wave. The basic difference of the formulation of the phase tracking equation in this case versus the top cladding case is that both reflecting interfaces are low-to-high index, so a π phase shift is acquired at both ϕ_{r1} and ϕ_{r2}. In the top cladding case, only one of the reflections gives a π phase shift.

2.7 Composite Bias

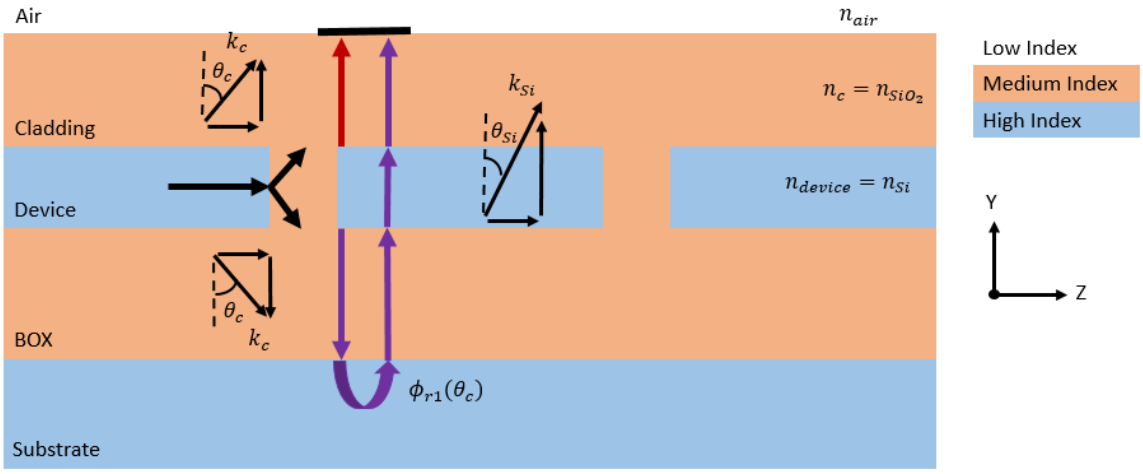

Figure 2.6: Upward Bias Diagram
Upward bias of the composite structure set by asserting coherence between BOX-substrate reflections and the air radiation mode at θ_d.

$$F(\theta_c, t_{BOX}, t_{device}) = 2\pi f \qquad (Equation\ 2.14)$$

$$F(\theta_c, t_{BOX}, t_{device}) = 2k_c \cos(\theta_c)\, t_{BOX} + \phi_{r1}(\theta_c) + k_{si} \cos(\theta_{Si})\, t_{device} \qquad (Equation\ 2.15)$$

$$\theta_{Si} = \arcsin\left(\frac{n_c}{n_{device}} sin(\theta_c)\right) \qquad (Equation\ 2.16)$$

$$F(\theta_c, t_{BOX}, t_{device}) = 2k_c \cos(\theta_c)\, t_{BOX} + k_{si} \cos(\theta_{Si})\, t_{device} + \pi \qquad (Equation\ 2.16)$$

The final phase matching goal is used to link the device layer thickness to a beneficial resonance behavior. With a "composite upward bias," we are asserting that the down-radiated plane wave at θ_c will have a reflection component from the BOX-substrate interface that is in phase with the up-radiated plane wave at θ_c. We are able to track phase by only using the y-directed component of the k-vectors in each medium because the z-directed component always remains the same, even after refraction at the SiO_2-Si interfaces. This is because Snell's Law can be seen to follow from the equality of the incident and transmitted waves' k-space parallel to the separating interface. Since

the length of the k-vector on either side of the interface is pre-determined by refractive index, the wave transmit angle has to adjust itself to make the interface-parallel components both k-vectors equal. Additionally, since both waves will travel through the top cladding, the phase gained in that region will cancel. This is why there is not actually a t_{clad} dependency in the final expression for F.

In a similar manner, a phase parameter could be derived that asserts that the cladding-air reflections are out-of-phase with the substrate radiation mode. This parameter would be explicitly dependent on t_{clad} and t_{device}, but not on t_{BOX}. If this phase parameter is called g, then its phase tracking function G tries to equal $2\pi g - \pi$. This phase parameter g can be expressed in terms of the other phase parameters using equation 2.17, printed below.

$$g = p + f - q + 1 \qquad (Equation\ 2.17)$$

When g is an integer value, it means that the cladding-air reflections are out of phase with the substrate mode, while when g is a half integer value, it means that the cladding-air reflections are in phase with the substrate mode. This follows the same convention as the other phase parameters – beneficial resonance conditions are represented by integer values of the phase parameter, while harmful resonance conditions are represented by half integer values. It is plain to see that if p, f, and q are integer values, then g will also be an integer value.

2.8 Compiled Model

Condition	Phase Equation
Grating Out-Radiation	$M(\theta_c, \beta_{eff}, \Lambda) = \beta_{eff}\Lambda - k_c \sin(\theta_c)\,\Lambda = 2\pi m$
Grating Back-Reflection	$N(\beta_{eff}, \Lambda) = 2\beta_{eff}\Lambda = 2\pi n - \pi$
Cladding Resonance	$P(\theta_c, t_{clad}) = 2k_c \cos(\theta_c)\, t_{clad} + \pi = 2\pi p$
BOX Resonance	$Q(\theta_c, t_{BOX}) = 2k_c \cos(\theta_c)\, t_{BOX} + 2\pi = 2\pi q - \pi$
Composite Radiation Bias	$F(\theta_c, t_{BOX}, t_{device}) = 2k_c \cos(\theta_c)\, t_{BOX} + k_{si} \cos(\theta_{Si})\, t_{device} + \pi = 2\pi f$ $g = p + f - q + 1$

Table 2.2: Compiled Phase Equations
Phase equations with reflection based phase shifts explicitly noted.

Table 2.2 is a compilation of the phase functions derived in sections 2.3-2.7. With this set of equations, we can choose a value for the free space decoupling angle θ_d, then walk it back to a cladding decoupling angle θ_c with Snell's Law. Then, if we assert integer values for *m*, *n*, *p*, *q*, and *f*, we will be able to solve for $t_{clad}, t_{BOX}, t_{device}, \Lambda$, and β_{eff}. Next, we can use t_{device} to numerically solve for the propagation constant of the Si waveguide segments, β_{device}. Finally, with $\beta_{device}, \beta_{eff}$, and Λ, we can find the fill factor ff, and then the etch length, l_{etch}. This sequence of equations is given in the equation set 2.18 – 2.21.

Equation 2.18 allows us to determine the mode angle, θ_0, of the dominant mode in the device layer. In this equation, $\phi_r(n_{Si}, n_{SiO_2}, \theta_0)$ is the Fresnel reflection phase shift gained from TIR. This reflection phase will be negative, which will allow valid solutions for positive device thicknesses. Equation 2.19 gives the propagation constant β_{device} that follows from θ_0. Equation 2.20 gives the fill factor in terms of all the device

layer propagation constants, where β_{etch} is equivalent to k_c. Lastly, fill factor can be used in equation 2.21 to get l_{etch}.

$$2k_{Si}\cos(\theta_0)t_{device} + 2\phi_r(n_{Si}, n_{SiO_2}, \theta_0) = 0 \qquad (Equation\ 2.18)$$

$$\beta_{device} = k_{Si}\cos(\theta_0) \qquad (Equation\ 2.19)$$

$$ff = \frac{\beta_{eff} - \beta_{device}}{\beta_{etch} - \beta_{device}} \qquad (Equation\ 2.20)$$

$$l_{etch} = ff * \Lambda \qquad (Equation\ 2.21)$$

3. GRATING MODEL IMPLEMENTATION

In section 2, a high level model for a full etch, constant pitch grating was derived by asserting spatial phase relationships between points in a subset of the device's fields. The resulting system of equations can be solved for an infinite number of combinations of the integer phase parameters *m, n, p, q,* and *f,* where each unique combination is defined as a "device mode." Some of these device modes will result in fabrication parameters that are not realizable because they are negative valued or potentially too small. Other device modes will result in fabrication parameters that are buildable, but that would give a device that is much too large, or that violates some design constraint or some implicit limit of our phase tracking functions.

In this section, we will first lay out the logical limits and design constraints for our device's fabrication parameters, and then we will discuss a Python based "Grating Designer" GUI that was developed to allow gratings to be interactively designed using the device modes model. In discussing the GUI, we will see that a full integer *m-n-p-q-f* device mode is not obtainable due to our design constraints, and so in the following subsection we will discuss how to strategically de-tune the phase parameters of the device modes model so that it satisfies our design constraints.

3.1 Device Limits

Parameter	Min	Max
t_{device}	0.1 μm	0.5 μm
t_{BOX}	0.7 μm	2 μm
t_{clad}	0	3 μm
l_{etch}	40 nm	–
Λ	0	1.5 μm
$Aspect$	0.3	0.5
$Mode\ Cutoff\ Number\ h$	–	0.9

Table 3.1: Logical Device Limits

$$aspect = \frac{l_{etch}}{t_{device}} \qquad (Equation\ 3.1)$$

$$2k_{Si}\cos(\theta_{crit})\,t_{device} + 2\phi_r\left(n_{Si}, n_{SiO_2}, \theta_{crit}\right) = 2\pi h \qquad (Equation\ 3.2)$$

Logical device limits for our full etch, constant pitch grating are tabulated in table 3.1. Device thickness and BOX thickness are fabrication limited parameters, and their limits are set by the ranges of thickness offered by our SOI platform vendor, SOITEC. The etch length is also a fabrication limited parameter, and it has a minimum of 40nm, which can be achieved by electron beam lithography. Additionally, the upper cladding thickness is fabrication limited to 3 μm because it is harder to accurately control the thickness of thicker films.

Grating period length (Λ) and two new parameters called *aspect* and *mode cutoff number* are our performance limited parameters. We want to keep Λ as short as possible because it will increase the resolution of our phased array of apertures, giving our out-radiated beam a more uniform phase front. We also want to limit it to under 1.5 μm

because the single mode fiber's mode field diameter is only $10.4\ \mu m$, so the 6-7 apertures resulting from a $1.5\ \mu m$ period length will work, but still might be too coarse.

Aspect is perhaps the most useful parameter for finding usable device modes, and again for tuning the de-coupling angle of those device modes. It is defined in equation 3.1 as the ratio between etch length and device layer height, so it quantifies the shape of the etch region. An aspect that is less than 1 will correspond to an etch region that looks like a tall and skinny rectangle in the Y-Z cross section. If we consider the angular space visible from the center point of a radiating aperture, having a small aspect will mean that most of the angular space is occupied by the input aperture to the next waveguide segment. In this sense, aspect is directly related to how much power remains in the device layer at each successive aperture. This also means that it is inversely related to how much power is radiated away from the device layer at each aperture. From experiment with simulation, aspects in the range of $0.3 - 1.0$ have resulted in devices that are efficient out-radiators, but that also do not out-radiate so much from one aperture that the subsequent apertures receive no power.

Mode number is the final performance limit, and it is used to ensure that the device layer height impressed by the device modes model will not result in a multi-mode waveguide. To ensure that it is strictly single mode, we will keep the cutoff mode number less than 1. At a mode number less than 1, the dominant mode will occur with mode number 0 at some angle larger than critical angle θ_{crit}, but the self-supporting mode with mode number 1 will occur with an angle less than θ_{crit}, and will thus be

leaky. Equation 3.2 can be solved to find the cutoff mode number *h* of the core Si waveguide.

3.2 Grating Designer

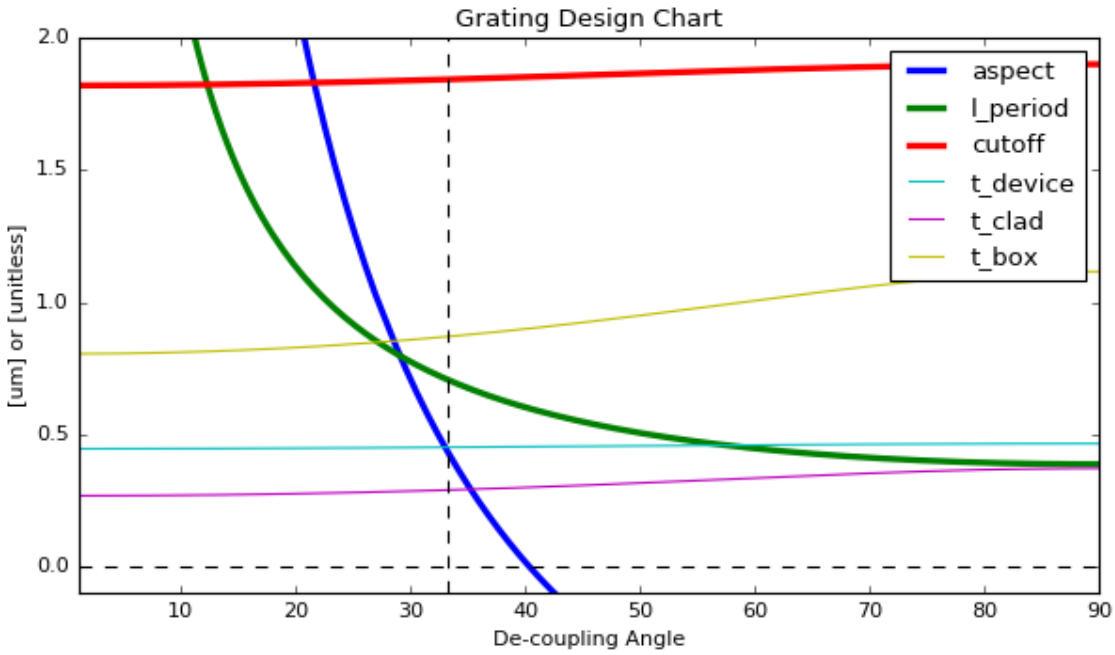

Figure 3.1: Grating Design Chart Example

To allow for rapid filtering of devices created by the device modes model, an interactive GUI was designed in Python using the *PyQT*, *numpy*, and *matplotlib* packages. The user is given a set of sliders that control the value for the *m, n, p, q,* and *f* phase parameters, and the device modes model is solved at the given settings for the full range of free space decoupling angles.

Figure 7 is a screenshot of the plot that is live-updated for the user. When a different *'mnpqf'* device mode is selected, the family of curves in figure 3.1 is instantaneously updated. The user can then examine the family of curves and determine

if there is a specific decoupling angle that would produce a device that satisfies the device limits discussed in section 3.1. If there is an angle that seems to work, the user can select that angle using yet another slider, and then export the resulting device parameters to FIMMWAVE for a rigorous coupled-mode analysis simulation.

For the specific device mode in figure 3.1, a 33º free space decoupling angle is selected for an *m-n-p-q-f* device mode of *1-4-1-3-3*. This selection has an aspect of 0.445, a period length of $0.71\ \mu m$, and a cutoff mode number of 1.8. Following our limits, this satisfies the aspect and the period length constraints, but it fails the single-mode constraint since the cutoff mode number is larger than 1. It turns out that a full integer set of the *m, n, p, q,* and *f* phase parameters is not capable of returning a device that satisfies the single mode condition. This will be expanded upon more in section 3.3.

Parameter	Value
t_{device}	$0.452\ \mu m$
$t_{cladding}$	$0.290\ \mu m$
t_{BOX}	$0.870\ \mu m$
l_{ridge}	$0.509\ \mu m$
l_{etch}	$0.201\ \mu m$
Λ	$0.71\ \mu m$
$aspect$	0.445
$cutoff$	1.8

Table 3.2: Physical Parameters for Example Device
Physical parameters for *m-n-p-q-f* device mode of 1-4-1-3-3 at 33^0.

For now though, we will continue with the example and export the current device (listed in table 3.2) to FIMMWAVE. FIMMWAVE will perform a rigorous analysis of the device, then return the calculated electric and magnetic fields to Python. A color mesh of each of the calculated fields can be overlaid on a plot of the device, as shown by the E_x and time average intensity fields in figure 3.2. If the fields look satisfactory; i.e.

the simulation looks like it executed successfully, then a coupling report can be generated at the click of a button.

The coupling report calculates the coupling efficiency between the dominant mode of the device layer waveguide and the dominant mode in a standard single mode fiber (SMF-28). It also reports on the loss mechanisms of the grating. Loss from the grating occurs in four basic forms. The first is back reflection, which is simply the fraction of the incident mode that is reflected back from the grating. The second is through loss, which is the fraction of the incident mode that does not decouple nor reflect, but continues to propagate in the device layer after the grating has ended. The third is downward loss, which is the fraction of the incident mode that decouples into a substrate radiation mode. The last form of loss is mode mismatch loss, which is the fraction of the incident mode that decouples into free space, but that misses the fiber due to the upward decoupled mode profile being a different shape than the fiber mode profile.

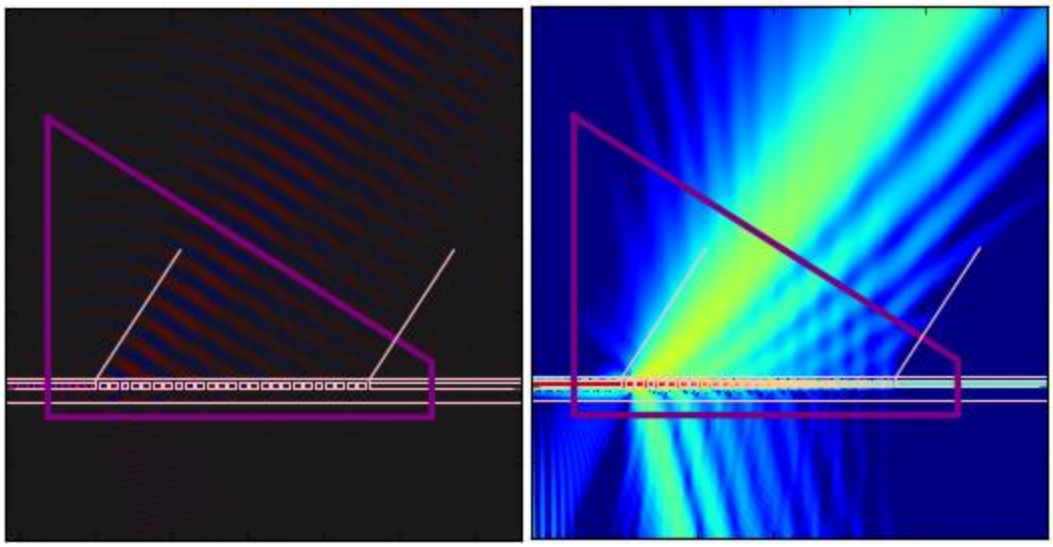

Figure 3.2: Python Field Graphics for Example Device
E_x (left) and time average intensity (right) fields overlaid on Y-Z cross section of the grating device. Lines extending upward and away from the device show the decoupling angle asserted by the device modes model. Purple enclosing box shows the boundaries for the coupling calculations.

The coupling report generates these efficiency and loss numbers by drawing a boundary around the grating and calculating the inward and outward Poynting vector along the boundary (Figure 3.2). The only input power comes from the dominant mode of the device layer waveguide, so the outward power at each of the four interfaces is compared to this input power to generate the report. The mode overlap integral is also calculated for the outward power along the upper slanted boundary of the calculation region. This boundary is automatically oriented so that the decoupled beam is normally incident. Figure 3.3 shows the power cross section of the upper boundary, and also shows the mode profile of SMF-28, aligned for maximum mode overlap.

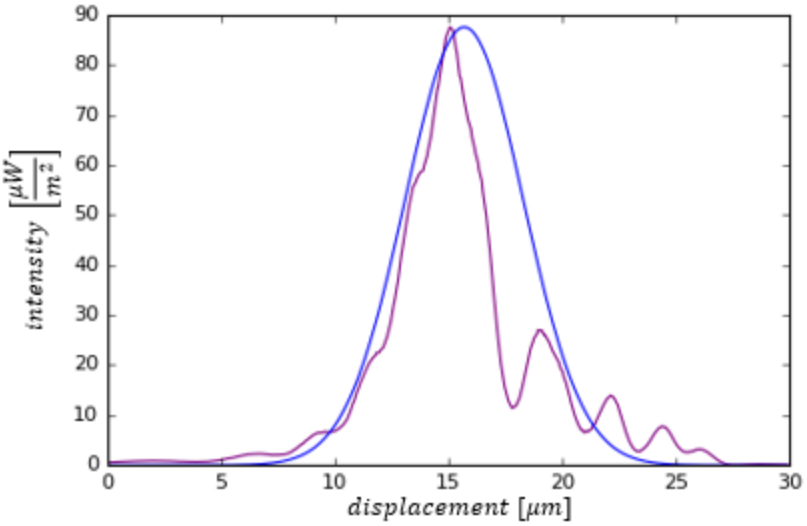

Figure 3.3: Mode Overlap for Example Device
Upward radiated power profile (purple) vs SMF-28 mode profile (blue). Max overlap efficiency calculated at 72.76%.

Parameter	Percent	dB
$Reflection\ Loss$	20.2 %	$-6.95\ dB$
$Through\ Loss$	10.5 %	$-9.79\ dB$
$Substrate\ Loss$	15.5 %	$-8.10\ dB$
$Mode-Mismatch\ Loss$	12.1 %	$-9.17\ dB$
$Coupling\ Efficiency$	32.5 %	$-4.88\ dB$

Table 3.3: Coupling Report for Example Device
Percent and dB figures are all with respect to input power.

The full coupling report for this example device is tabulated in table 3.3. A -4.88 dB coupler results from this specific device, however the device is not single mode. The higher order mode is coupled to in the latter segments of the grating due to mode expansion of the input mode in the etched regions. This higher order mode may be a source of loss for this grating, as the phase parameters are only calibrated for the dominant mode.

3.3 De-Tuning the Device Modes Model

Since there is not a full integer device mode that satisfies the constraint for maintaining a single mode device layer, one or a few of the phase parameters have to be relaxed to non-integer values. The phase parameters are defined to optimize interference patterns at integer values, so it follows that when they take on half integer values, their resonance behavior will be reversed – constructive interference will turn into destructive interference, and vice-versa. With this knowledge, we can identify which phase parameters control the device layer thickness, and then de-tune them in such a way as to minimize their effect on coupling efficiency.

The phase parameters that can control device thickness are the *q* and *f* parameters. In the solution to the device modes model, the *q* parameter is directly related to the buried oxide thickness, while the *f* parameter sets device thickness based on where *q* set the buried oxide thickness. From tuning, it turns out that in order to bring the device layer thickness into the single mode range, we need to give up exactly a half integer from *q* and *f*, collectively. This means it can all come out of *q*, or all come out of *f*, or part can come out of both. Devices tuned for the same de-coupling angle were tested with all of the half integer coming out of *q*, all of the half integer coming out of *f*, and half of the half integer coming out of both *q* and *f*. The *m*, *n*, and *p* parameters were held constant for each of these tests, so the only physical parameter changing was the buried oxide thickness, as shown in table 3.4.

Parameter	Value
t_{device}	$0.225\ \mu m$
$t_{cladding}$	$0.574\ \mu m$
t_{BOX}	$variable$
l_{ridge}	$0.591\ \mu m$
l_{etch}	$0.169\ \mu m$
Λ	$0.76\ \mu m$
$aspect$	0.75
$cutoff$	0.92

Table 3.4: Physical Parameters of De-Tuned Devices

Parameter	$\boldsymbol{q = 4}$ $\boldsymbol{f = 4.5}$	$\boldsymbol{q = 4.25}$ $\boldsymbol{f = 3.75}$	$\boldsymbol{q = 4.5}$ $\boldsymbol{f = 4}$
$Reflection\ Loss$	15.8 %	15.8 %	14.5 %
$Through\ Loss$	22.4 %	13.1 %	9.9 %
$Substrate\ Loss$	30.8 %	24.4 %	16.6 %
$Mode - Mismatch\ Loss$	4.3 %	6.3 %	10.2 %
$Coupling\ Efficiency$	15.8 %	35.7 %	44.2 %

Table 3.5: Coupling Report for De-Tuned Devices

Table 3.5 gives the coupling report for each of these *q* and *f* combinations. It turns out that the *f* parameter is much more important than the *q* parameter for coupling efficiency. This means it is more important to maintain coherence between BOX-substrate reflections and the decoupled radiation mode than it is to assert a self-destructing mode in the BOX layer with the *q* parameter. Keeping the *f* parameter at an integer value while setting the *q* parameter to a half integer value results in the best device.

A similar weighting principal applies to *p* and its equivalent *f* parameter, *g*. The phase parameter *p* was set to a half integer value because it enables the phase parameter *g* to take on a full integer value (Equation 2.17). When *g* takes on a full integer value, it asserts the cladding-air reflections to be fully out of phase with the substrate radiation

mode. Since *p* is a half integer value, the cladding resonance condition is not optimized, but maintaining a destructive relationship in the substrate between cladding-air reflections and the initial device layer leakage was found to be much more important. This is why the

4. RESULTS

The optimized full etch, constant pitch grating design is presented in this section. The device achieves a coupling efficiency of -3.55 dB to SMF-28 optical fiber at a free-space decoupling angle of 29.47^{o}. The time average intensity color mesh from the Python and FIMMWAVE simulation environment is plotted in figure 4.1, along with mode overlap cross section of the ejected beam. Table 4.1 lists the detailed coupling efficiencies and loss figures of the device. Table 4.2 lists the fabrication parameters. Last, table 4.3 gives the device modes model parameters.

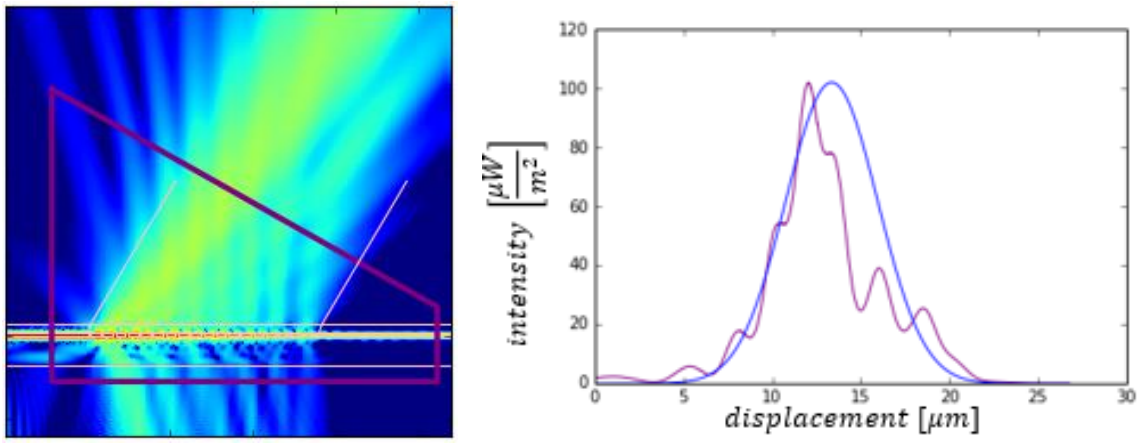

Figure 4.1: Python Simulation Graphics for Optimized Device
On the left, the time average intensity is overlaid on the physical grating. On the right, the up-ejected intensity cross section is plotted (purple), along with the optimally aligned mode profile of SMF-28 (blue).

Parameter	$Percent$	Db
$Reflection\ Loss$	14.5 %	$-8.39\ dB$
$Through\ Loss$	9.9 %	$-10.04\ dB$
$Substrate\ Loss$	16.6 %	$-7.80\ dB$
$Mode-Mismatch\ Loss$	10.2 %	$-12.01\ dB$
$Coupling\ Efficiency$	44.2 %	$-3.55\ dB$
$Ejection\ Efficiency$	63.5 %	$-1.97\ dB$
$Upward\ Bias$	76.6 %	–
$Downward\ Bias$	23.4 %	–
$Mode\ Overlap$	81.2 %	–

Table 4.1: Detailed Coupling Report for Optimized Device
Decibel values are only given for efficiencies/losses taken with respect to input power.

Parameter	Value
t_{device}	$0.225\ \mu m$
$t_{cladding}$	$0.574\ \mu m$
t_{BOX}	$1.721\ \mu m$
l_{ridge}	$0.591\ \mu m$
l_{etch}	$0.169\ \mu m$
Λ	$0.76\ \mu m$
$N_{periods}$	18
$l_{grating}$	$13.68\ \mu m$
$aspect$	0.75
$cutoff$	0.92
$Simulated\ \theta_d$	30.67^0

Table 4.2: Physical Parameters for Optimized Device

Parameter	Value
$Asserted\ \theta_d$	29.47^0
m	1
n	4
p	1.5
q	4.5
f	4
g	1

Table 4.3: Device Modes Model Parameters for Optimized Device

In Table 4.1, the parameters up to coupling efficiency have been explicitly defined on page 25. The remaining parameters are ejection efficiency, upward and downward bias, and mode overlap. Ejection efficiency is the fraction of input power that is radiated up and down away from the grating. Upward and downward bias is the fraction of ejected light in the upward and downward direction, respectively. Mode overlap remains as the raw overlap of the upward radiation pattern with SMF-28 single mode fiber (10.4 μm MFD).

As discussed in section 3.3, the optimized design must relax a set of the phase parameters to achieve single mode operation in the device layer. The phase parameters p and q are both relaxed by a half integer to optimally achieve this effect. This allows the phase parameters f and g to remain as integer values. The insight gained here is that it is more important to assert a composite upward bias than it is to assert beneficial resonance conditions in the leaky modes of the top cladding or buried oxide layers.

In Table 4.2, the physical parameters for the optimized device are tabulated. The device thickness and BOX thickness are both within the limits provided by the SOI platform from SOITEC, and the device thickness is also small enough that only the dominant mode propagates. Further, the period length Λ is favorably small at 760 nm, and these periodic sections are repeated 18 times to stretch the total grating length to 13.68 μm. The etch length for this device is 169 nm, and this feature is easily achieved by electron beam lithography. It is also feasibly achieved by modern projection optical lithography systems.

To expand the beam in the X-direction, the grating device must be approximately 10 μm wide. An adiabatic taper must be fabricated to join the photonic integrated circuit waveguides to the grating structure. The main characteristic of an adiabatic taper is that the dominant mode in the small width and large width waveguides that it joins are coupled with high efficiency. These devices are well documented for SOI.

5. SUMMARY

A design process for full etch, constant pitch grating couplers with upper cladding was developed in detail by defining a set beneficial resonance conditions over the k-space of a subset of the grating's fields. Solutions to the system of equations resulting from these resonance conditions were modal in nature, and could be solved for an infinite number of combinations of their governing phase parameters. An interactive, Python based GUI environment was created to aid in filtering to valid, and then optimal, "device mode" solutions.

For valid device mode solutions, there was high agreement found between the asserted and simulated decoupling angle. Further, it was observed that it is more important for optimization to assert that reflections from the BOX-substrate interface are in phase with the out-radiated air mode, than to assert that the BOX layer thickness results in low resonance for its leaky mode. A similar observation occurs for the cladding-air interface reflections, which should be out of phase with the radiation mode in the substrate before the top cladding thickness results in high resonance for its leaky mode.

This high level process was applied to optimize a full etch, constant pitch grating coupler with top cladding oxide over a commercially available Silicon-on-Insulator platform from SOITEC. At an operating wavelength of 1550nm, the optimized device achieves a -3.55 dB coupling efficiency between the dominant TE mode of its strictly single mode input waveguide and a SMF-28 single mode optical fiber, through a free space decoupling angle of 29.47^0.

REFERENCES

[1] Antelius, Mikael, Kristinn B. Gylfason, and Hnas SohlstrÃ¶m. "An Apodized SOI Waveguide-to-fiber Surface Grating Coupler for Single Lithography Silicon Photonics." *Optics Express* 19.4 (2011): 3592. Web.

[2] Ding, Yunhong, Haiyan Ou, and Christophe Peucheret. "Ultrahigh-efficiency Apodized Grating Coupler Using Fully Etched Photonic Crystals." *Optics Letters* 38.15 (2013): 2732. Web.

[3] Halir, R., P. Cheben, J. H. Schmid, R. Ma, D. Bedard, S. Janz, D.-X. Xu, A. Densmore, J. Lapointe, and Ã• . Molina-FernÃ¡ndez. "Continuously Apodized Fiber-to-chip Surface Grating Coupler with Refractive Index Engineered Subwavelength Structure." *Optics Letters* 35.19 (2010): 3243. Web.

[4] Wang, Yun. *Grating Coupler Design Based on Silicon-on-insulator*. Thesis. Vancouver / The University of British Columbia, 2013. N.p.: n.p., n.d. Web. <https://open.library.ubc.ca/cIRcle/collections/ubctheses/24/items/1.0073806>.

[5] Zhong, Qiuhang, Venkat Veerasubramanian, Yun Wang, Wei Shi, David Patel, Samir Ghosh, Alireza Samani, Lukas Chrostowski, Richard Bojko, and David V. Plant. "Focusing-curved Subwavelength Grating Couplers for Ultra-broadband Silicon Photonics Optical Interfaces." *Optics Express* 22.15 (2014): 18224. Web.